Applied Catalysis B: Environmental 306 (2022) 121111

Contents lists available at ScienceDirect

Applied Catalysis B: Environmental

journal homepage: www.elsevier.com/locate/apcatb

Protecting the state of Cu clusters and nanoconfinement engineering over hollow mesoporous carbon spheres for electrocatalytical C-C coupling

Yue Pan [a], Hongdong Li [a], Juan Xiong [a], Yaodong Yu [a], Haoyang Du [a], Shaoxiang Li [b], Zhanchao Wu [a], Suping Li [c], Jianping Lai [a,*], Lei Wang [a,b,**]

[a] Key Laboratory of Eco-chemical Engineering, Key Laboratory of Optic-electric Sensing and Analytical Chemistry of Life Science, Taishan Scholar Advantage and Characteristic Discipline Team of Eco-Chemical Process and Technology, College of Chemistry and Molecular Engineering, Qingdao University of Science and Technology, Qingdao, PR China

[b] Shandong Engineering Research Center for Marine Environment Corrosion and Safety Protection, College of Environment and Safety Engineering, Qingdao University of Science and Technology, Qingdao 266042, PR China

[c] Library, Qingdao University of Science and Technology, Qingdao 266042, Shandong, PR China

ARTICLE INFO

Keywords:
CO_2RR
Copper
Nanoclusters
HMCSs
C_2 selectivity

ABSTRACT

Copper-based catalysts are widely used to adjust the activity and selectivity of CO_2 electroreduction reactions (CO_2RR). In this article, we choose to use hollow mesoporous carbon spheres (HMCS) to confine and protect Cu clusters to achieve high C_2 selectivity. The electrocatalytic results show that when the amount of Cu clusters confined by HMCS reaches 20% (Cu/HMCS$_5$-20%), the selectivity of C_2 products reach 88.7% at − 1.0 V vs. RHE. *In situ* Fourier transform infrared spectroscopy (FTIRS) shows that Cu clusters confined and protected by HMCS is beneficial to the conversion of *CO to *CHO, while the nanocavities formed by HMCS can effectively confine the in situ formed *CHO carbon intermediates, which facilitates the C-C bond coupling to form C_2H_4 and C_2H_5OH. We proposes a method to improve the C_2 selectivity of CO_2RR and reduce the amount of Cu in CO_2RR by using the confinement effect of HMCS.

1. Introduction

The roadmap for achieving carbon neutrality with excess renewable electricity has attracted people's attention [1–16]. So far, Cu-based catalysts have shown great potential in the electrochemical reduction of carbon dioxide (CO_2) to synthesize high-value multi-carbon (C_+) products [17–40]. However, the selectivity and activity of Cu materials for electrocatalytic carbon dioxide reduction reaction (CO_2RR) are often difficult to control. The main obstacle to obtaining high value-added products from carbon dioxide is the coupling of C—C bonds. In order to improve the selectivity and stability of CO_2RR, the application and protection of different copper sites in CO_2RR have been extensively studied [19,41–47]. For example, Gong et al. described the controllable construction of Cu^0-Cu^+ sites derived from the well-dispersed cupric oxide supported on copper phyllosilicate lamella to enhance CO_2RR performance [41]. Xia et al. proved that controlling the surface oxidation of copper nanowires to form a relatively thick and smooth oxide sheath can greatly improve its C_{2+} selectivity and stability [42]. Sargent et al. using boron to adjust the ratio of $Cu^{\delta+}$ to Cu^0 active sites and protect the copper sites, it was found that the C_2 Faraday efficiency (FE) was 79.2% [43]. The reported results are not satisfactory, so it is considered to introduce a confinement effect to protect the copper sites and reduce the loss of carbonaceous intermediates, thereby increase the coupling of C-C bonds and improve the C_2 selectivity.

Recent studies have used limiting effects to enhance the selectivity of CO_2RR for multi-carbon products [48–50]. Gao et al. reported a Cu catalyst with nanocavities that can confine the carbon intermediates formed in situ and stabilize the copper species. The experimental results show that the experimental measurement on the multi-hollow cuprous oxide catalyst shows that the C_2 Faraday efficiency is 75.2 ± 2.7% [48]. Sargent et al. developed a method to synthesize an open Cu nanocavity structure with adjustable geometry by electroreduction of Cu_2O cavities

* Corresponding author.
** Corresponding author at: Key Laboratory of Eco-chemical Engineering, Key Laboratory of Optic-electric Sensing and Analytical Chemistry of Life Science, Taishan Scholar Advantage and Characteristic Discipline Team of Eco-Chemical Process and Technology, College of Chemistry and Molecular Engineering, Qingdao University of Science and Technology, Qingdao, PR China.
E-mail addresses: jplai@qust.edu.cn (J. Lai), inorchemwl@126.com (L. Wang).

https://doi.org/10.1016/j.apcatb.2022.121111
Received 2 December 2021; Received in revised form 6 January 2022; Accepted 17 January 2022
Available online 19 January 2022

formed by acid corrosion. During the electroreduction process of carbon monoxide, the FE of propanol can reach 21 ± 1% [49]. These reports all use etched Cu nanocavities to achieve the confinement effect, but the amount of Cu is very large and does not achieve the desired C_2 selectivity. The nanopore channels of hollow mesoporous carbon spheres (HMCS) can effectively confine and protect the clusters, and provide a nanocavity with confinement effect [51]. Therefore, we consider using HMCS to protect Cu clusters and provide a confinement effect to increase the C_2 selectivity of CO_2RR and reduce the amount of Cu.

Here, we further apply the confinement effect to enhance the production of C_2. Firstly, the pore size of the hollow mesoporous carbon spheres was adjusted and 5 nm and 10 nm pore sizes were synthesised. After finding the best pore size, the loading of the clusters was adjusted to 10%, 20% and 30% Cu clusters respectively. The material with the best C_2 selectivity to CO_2RR was found by optimizing the loading of Cu clusters. The 5 nm pore sizes HMCS was loaded with 10%, 20% and 30% Cu clusters and named Cu/$HMCS_5$-10%, Cu/$HMCS_5$-20% and Cu/$HMCS_5$-30%, respectively. The electrocatalytic measurements showed confinement effects in terms of activity and selectivity of the CO_2RR. The C_2 Faraday efficiency (FE) of Cu/$HMCS_5$-20% at − 1.0 V vs. the reversible hydrogen electrode (RHE) is higher than most existing reports.

2. Experimental section

2.1. Materials synthesis

2.1.1. Synthesis of 5 nm and 10 nm pore size hollow mesoporous carbon spheres

The synthesis was performed according to the method of Lou et al. [52]. Generally, 70 mL of ethanol, 10 mL of deionized water and 3.0 mL of ammonium hydroxide are stirred together at room temperature for 10 min, and then 3.5 mL of Tetrapropyl orthosilicate (TPOS) is added to the solution under stirring. After 15 min, 2.0 mL of a freshly prepared ethanol solution of resorcinol (0.4 g) and 0.56 mL of formaldehyde (37 wt%) were added to the solution. After stirring for 24 h at room temperature, the silica@silica/RF nanospheres were collected by centrifugation, washed with ethanol several times, and then dried at 60 °C under vacuum overnight. Then, put the silica@silica/RF in a porcelain boat. After annealing for 4 h at 700 °C (2 °C min^{-1}) in N_2 atmosphere, silica@silica/carbon was obtained. The obtained silica@silica/carbon was etched with 1.0 M sodium hydroxide at 70 °C for 24 h to obtain HMCS [51]. The hollow carbon spheres were collected by centrifugation, washed with deionized water and ethanol several times, and then dry under vacuum at 60 °C overnight for further use. HMCSs with pore size of 10 nm were synthesized with Tetraethyl orthosilicate (TEOS)/TPOS of 4/1 and ethanol/water of 60/20, respectively, while other conditions remain unchanged.

2.1.2. Synthesis of $Cu_{12}DT_8Ac_4$ clusters

The synthesis was performed according to the method of Wu et al. [53]. 30 mg (0.1 mmol) copper acetylacetonate was dissolved in a mixed solvent of 2 mL BE (dibenzyl ether) and 5 mL LP (liquid paraffin), and sonicated at room temperature for 10 min. 1 mL (4 mmol) of DT (dodecyl mercaptan) was added to the mixture as a ligand and reducing agent, and stirred at 30 °C for 1 min to produce DT-coated Cu clusters.

2.1.3. Synthesis of Cu/HMCS material

A predetermined amount of $Cu_{12}DT_8Ac_4$ clusters was dissolved in 1 mL of acetone and added dropwise to the suspension containing 10 mg of HMCS [23]. The loading method still follows the method of Lou et al. [52]. After stirring for 10 h under ambient conditions, use acetone to centrifuge and wash 3–5 times. The Cu/HMCS composite was collected by evaporating the solvent under vacuum, and then dried under vacuum at 60 °C overnight. Then the catalyst was annealed in Ar/H_2 (95/5) atmosphere at 350 °C to remove surface ligands and obtain Cu/HMCS electrocatalyst.

3. Results and discussion

3.1. Synthesis and structural characterization of Cu/HMCS

The effect of copper catalysts on CO_2RR selectivity has been extensively studied, but a method using hollow mesoporous carbon spheres to confine copper clusters has never been carried out. Here, a method is proposed to study copper-catalyzed CO_2RR selectivity/activity using hollow mesoporous carbon spheres confined copper clusters by adjusting the loading of Cu. The nanocluster catalyst materials were constructed by synthesising specific Cu nanoclusters and loading them into HMCS. The formation of HMCS carriers and the anchoring of metal atoms together ensure their compatibility throughout the reaction process. First, $Cu_{12}DT_8Ac_4$ nanoclusters were synthesised according to the method of Wu et al. As can be seen in Fig. S1, the successful synthesis of $Cu_{12}DT_8Ac_4$ nanoclusters was demonstrated by Matrix-Assisted Laser Desorption/ Ionization Time of Flight Mass Spectrometry (MALDI-TOF-MS) tests. Next, the HMCS with pore sizes of 5 nm and 10 nm were synthesised. As shown in Figs. S2 & S3, carbonised core-shell silicon@Si/resorcinol formaldehyde (SiO_2 @SiO_2/RF) nanospheres were first synthesised. Then the SiO_2 is removed from the material to obtain HMCS with pores of 5 nm and 10 nm as shown in Figs. S4 & S5. To demonstrate that the desired pore sizes were synthesised, the materials were subjected to Brunauer Emmett Teller (BET) testing as shown in Figs. S6 & S7, which were considered to be successfully synthesised with 5 nm and 10 nm pore size carbon spheres. The prepared HMCS and $Cu_{12}DT_8Ac_4$ clusters with different pore size were stirred, washed and calcined at room temperature to obtain Cu/$HMCS_5$-20% and Cu/$HMCS_{10}$-20% materials. The synthesised Cu/$HMCS_5$-20% materials were examined by Scanning electron microscopy (SEM) (Figs. S8a & S9), transmission electron microscopy (TEM) (Figs. 1a & S10a & S11), high-angle annular dark field-scanning transmission electron microscope (HAADF-STEM) (Fig. 1b & c), energy dispersive spectroscopy (EDS) mapping (Fig. 1d) and BET test (Fig S12). From the above characterization, the copper clusters were found to be homogeneously dispersed in HMCS and were considered to be successfully loaded onto HMCS. As can be seen in Fig. 1d & S13, there is a significant amount of oxygen and a small amount of S in the material, which is thought to be caused by the formation of CuO in air from unstable copper monoatoms after deliganding, and the small amount of S is thought to be normal for deliganding residues. SEM (Fig. S8b) and TEM (Fig. S10b) are used to prove that the Cu/$HMCS_{10}$-20% material had been successfully synthesized.

In order to better investigate the electronic structure of the synthesised Cu/$HMCS_5$-20% and Cu/$HMCS_{10}$-20% materials. The materials were characterised by X-ray photoelectron spectroscopy (XPS). The synthesised $Cu_{12}DT_8Ac_4$ clusters were first tested by XPS and Cu LMM Auger spectroscopy. As shown in Fig. S14, it can be seen that Cu(0)/Cu (I) can be seen co-existing in the Cu clusters. The synthesised Cu/$HMCS_5$-20% and Cu/$HMCS_{10}$-20% materials were later tested by XPS. As shown in Fig. S15, in the XPS spectra of the Cu/$HMCS_5$-20% and Cu/$HMCS_{10}$-20% materials, the peaks at 932.1 eV and 952.1 eV were attributed to the Cu(0)/Cu(I) 2p3/2 peak and the Cu(0)/Cu(I) 2p1/2 peak, respectively, while the peaks at 934.1 eV and 954.1 eV were attributed to the Cu(II) 2p3/2 and Cu(II)2p1/2. Cu(II) satellite peaks can also be observed in XPS spectra of the material. The Cu material should also be further analysed using the Cu LMM Auger spectrum, where the simultaneous presence of Cu(0)/Cu(I)/Cu(II) can be seen in Fig. S15b. As shown in Fig. 2a & S14a, compared with the XPS spectra of copper clusters, the ligands are removed after high-temperature annealing treatment, and the S element is significantly reduced. The clusters that lose the ligand protection are oxidized to produce CuO, mostly Cu(II) exists, which is the target product and is the same as the previous conclusion.

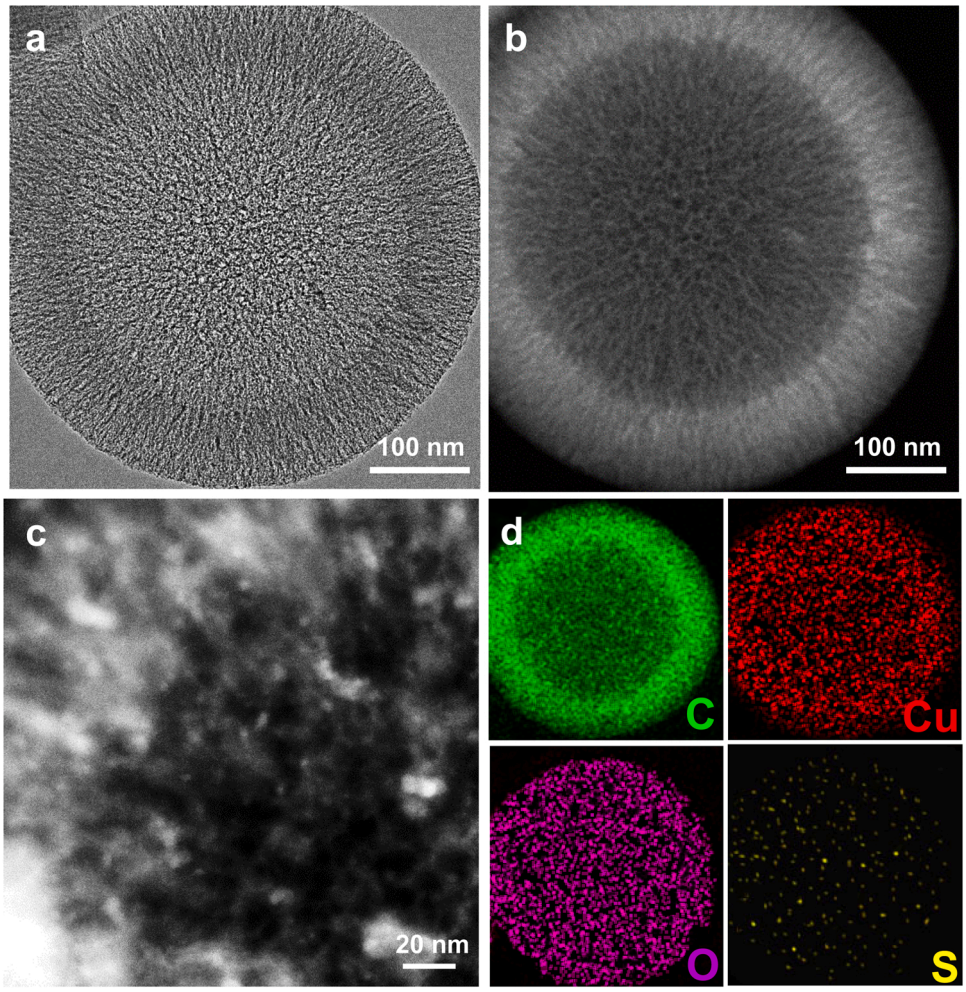

Fig. 1. (a) TEM (b, c) HAADF-STEM and (d) Mapping images of Cu/HMCS$_5$-20%.

The synthesised Cu/HMCS$_5$-20% and Cu/HMCS$_{10}$-20% materials were then tested in the flow cell (Fig. S16). Linear sweep voltammetry (LSV) curves were tested in 1 M KOH in both N_2 and CO_2 atmospheres (Fig. S17). The products were then obtained by 1 h current-time (i-t) testing in 1 M KOH saturated with CO_2 at different applied potentials (Fig. S18a & b). After collecting the liquid and gaseous products, they were detected by NMR spectroscopy and gas chromatography, respectively, after which the Faraday efficiencies of the different materials at different applied potentials and the current density/voltage diagrams of the different C_+ products were obtained using the Faraday formula (Eq. 1). Cu/HMCS$_5$-20% was found to have a higher C_2 selectivity compared to Cu/HMCS$_{10}$-20% (Fig. S18c & d).

Then, the 5 nm pore size HMCS was selected as the carrier and materials with different Cu cluster loadings were synthesised using the same method. The Cu cluster loadings of 10% and 30% were named Cu/HMCS$_5$-10% and Cu/HMCS$_5$-30%, respectively. The synthesised materials were first tested by SEM (Fig. S19), TEM (Fig. S20) and HAADF-STEM (Fig. S21). It was found that the materials with the same morphology as Cu/HMCS$_5$-20% were synthesized, but the Cu clusters in Cu/HMCS$_5$-30% underwent significant agglomeration compared to the other Cu clusters, which may have led to a reduction in the number of active sites and reduced nanocavity space in the Cu/HMCS$_5$-30% material. The energy dispersive X-ray spectroscopy (EDX) images (Fig. S22) showed that the synthesised Cu/HMCS$_5$-10% and Cu/HMCS$_5$-30% materials differ only in the Cu content compared to the Cu/HMCS$_5$-20% material, the difference in the content of O and S elements is not significant, so the main composition of the synthesised material is considered to be certain. The Cu content of the material was quantified by EDX (Fig. S13 & S22), XPS and ICP (Table S1), it was found that the synthesized material had the target Cu content. XRD tests were also carried out on the material (Fig. S23) and compared to the C standard card (PDF#41–1487) reflecting the major carbon carriers. The materials Cu/HMCS$_5$-10%, Cu/HMCS$_5$-20% and Cu/HMCS$_5$-30% were considered to have been successfully synthesised.

The materials were next analysed by XPS, as shown in Figs. 2a & S24, and three materials have less S elements and more O elements compared to the Cu clusters, thought to be the result of successful ligand removal. As shown in Fig. 2b, XPS spectra of Cu/HMCS$_5$-10%, Cu/HMCS$_5$-20% and Cu/HMCS$_5$-30% materials can be found at 932.1 eV and 952.1 eV attributed to the Cu(0)/Cu(I) 2p3/2 and Cu(0)/Cu(I) 2p1/2 peaks, respectively. Cu(II) 2p3/2 and Cu(II) 2p1/2 can be found at both 934.1 eV and 954.1 eV, respectively, and Cu(II) satellite peaks can also be observed. The Cu material should be further analysed using the Cu LMM Auger spectrum and the simultaneous presence of Cu(0)/Cu(I)/Cu(II) can be seen in Fig. 2c. This is the same conclusion as that obtained earlier, so it is considered that Cu/HMCS$_5$-10%, Cu/HMCS$_5$-20% and Cu/HMCS$_5$-30% materials have been synthesised, which are all identical except for the Cu content.

3.2. *Electrocatalytic performance of Cu/HMCS$_5$ with different Cu loading*

The electrochemical tests of the synthesised material will be carried out in the flow cell (Fig. S15). The LSV curves were first tested in 1 M KOH under N_2 atmosphere and CO_2 atmosphere to obtain a comparison

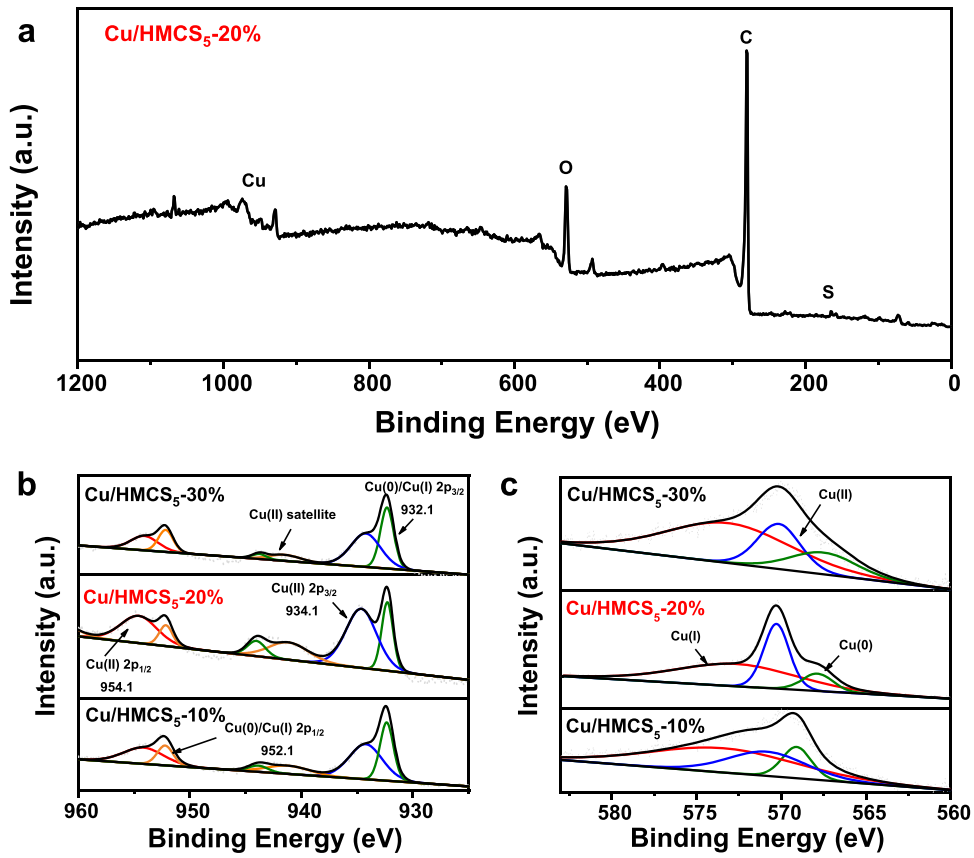

Fig. 2. (a) Survey XPS characterization of Cu/HMCS$_5$-20%. (b) Cu XPS characterization of the three synthetic materials. (c) LMM Auger spectrum test of the three synthetic materials.

of the LSV of the three materials in Figs. 3a & S25. The ECSA of Cu/HMCS$_5$-10% (22.5 cm^2), Cu/HMCS$_5$-20% (26.7 cm^2), Cu/HMCS$_5$-30% (24.8 cm^2) was calculated by recording CV curves in 1.0 M KOH at different scan rates from 20 to 100 mV s^{-1} (Fig. S26). By ECSA-normalised, the comparison reveals that Cu/HMCS$_5$-20% has the best current density at the same applied voltage(Fig. S27). The products were then obtained by current-time (i-t) testing in CO_2 saturated 1 M KOH at different application potentials for 1 h. The i-t tests for the three materials at different application potentials are shown in Figs. S18a & S28. After collecting the liquid and gaseous products, they were detected by NMR spectroscopy and gas chromatography respectively. The NMR images of the three materials are shown in Fig. S29 and the gas chromatography data are shown in Fig. S30. The FE of the different materials at different applied potentials and the current density/voltage plots of the different C_+ products were obtained using the Faraday equation (Eq. 1) and the results are summarised in Fig. 3. It can be seen that the materials show good catalytic activity for CO_2RR, with a large number of products detected for carbon monoxide (CO), methane (CH_4), formate, ethanol (C_2H_5OH), ethylene (C_2H_4) and hydrogen (H_2). Cu/HMCS$_5$-20% showed the best C_2 selectivity, with the highest C_2 FE of 88.7% at − 1.0 V vs. RHE, which is higher than Cu/HMCS$_5$-10% (69.3%) and Cu/HMCS$_5$-30% (80.1%) at the same applied voltage. The highest FE for C_2H_4 was 68.6%. As can be seen by Table S2, Cu/HMCS$_5$-20% materials had better C_2 FE in recent reports. The Cu cluster after removal of the ligand is considered to be more CuO and there is a synergy of Cu(0), Cu (I) and Cu(II) monoatoms. In contrast, Cu/HMCS$_5$-20% has more active sites and better confinement effects compared to Cu/HMCS$_5$-10% and Cu/HMCS$_5$-30%, resulting in better C_2 FE.

In order to show the long-term stability of the material, the 20 h current time (i-t) test was carried out. The long-term i-t and C_2 FE plots for Cu/HMCS$_5$-20% are shown in Fig. 3f. And the long-term i-t and C_2 FE plots for the Cu/HMCS$_5$-10% and Cu/HMCS$_5$-30% materials are shown in Fig. S31. It can be seen that the synthesised materials maintain a good product Faraday efficiency even at longer reaction times. SEM (Fig. S32) and TEM (Fig. S33) tests were carried out on the three materials after the reaction. It can be seen that the clusters in the materials did not change significantly after the electrochemical tests. In order to better observe the changes in the materials after the reaction, HADDF-STEM tests were carried out on the reacted Cu/HMCS$_5$-20% material. As shown in Fig. S34 it can be clearly seen that the Cu/HMCS$_5$-20% material did not change significantly in the internal Cu clusters before and after the reaction. To observe the change in Cu valence state after the reaction, the reacted material was tested by Cu XPS and Cu LMM Auger spectroscopy. As shown in Fig. 2 & Fig. S35, Cu(II) in Cu/HMCS$_5$-20% will be reduced at the beginning of the reaction [24,28,37]. It can be seen that the amount of Cu(II) is significantly decreased, and the corresponding Cu(0) & Cu(I) increased. However, by comparing the XPS of the material after 2.5 h (Fig. S36), 7.5 h (Fig. S37) and 20 h (Fig. S35) reactions, the amount of Cu(0), Cu(I) & Cu(II) in the catalyst was found to remain constant during the electrocatalytic process. After a long i-t test, it was found that the synthesised Cu materials did not undergo large changes from morphology and distribution to valence and electronic structure.

In order to better investigate the reaction process of the material, the in situ Fourier-transform infrared spectroscopy (FTIRS) tests were performed to characterise the reaction intermediates. Electrochemical tests were carried out from an applied voltage of − 0.8 V to − 1.2 V vs. RHE on Cu/HMCS$_5$-10% and Cu/HMCS$_5$-20%. As shown in Fig. 4, the peaks at 1250 cm^{-1}, 1334 cm^{-1}, 1400 cm^{-1} and 1565 cm^{-1} can be attributed to the stretching, symmetric stretching and asymmetric stretching of the OHC deformation-O for the *COOH intermediate, respectively, which is widely considered to be a key intermediate in the electroreduction of CO_2 to CO or CH_4 [54,55]. The peak at 2065 cm^{-1} can be attributed to

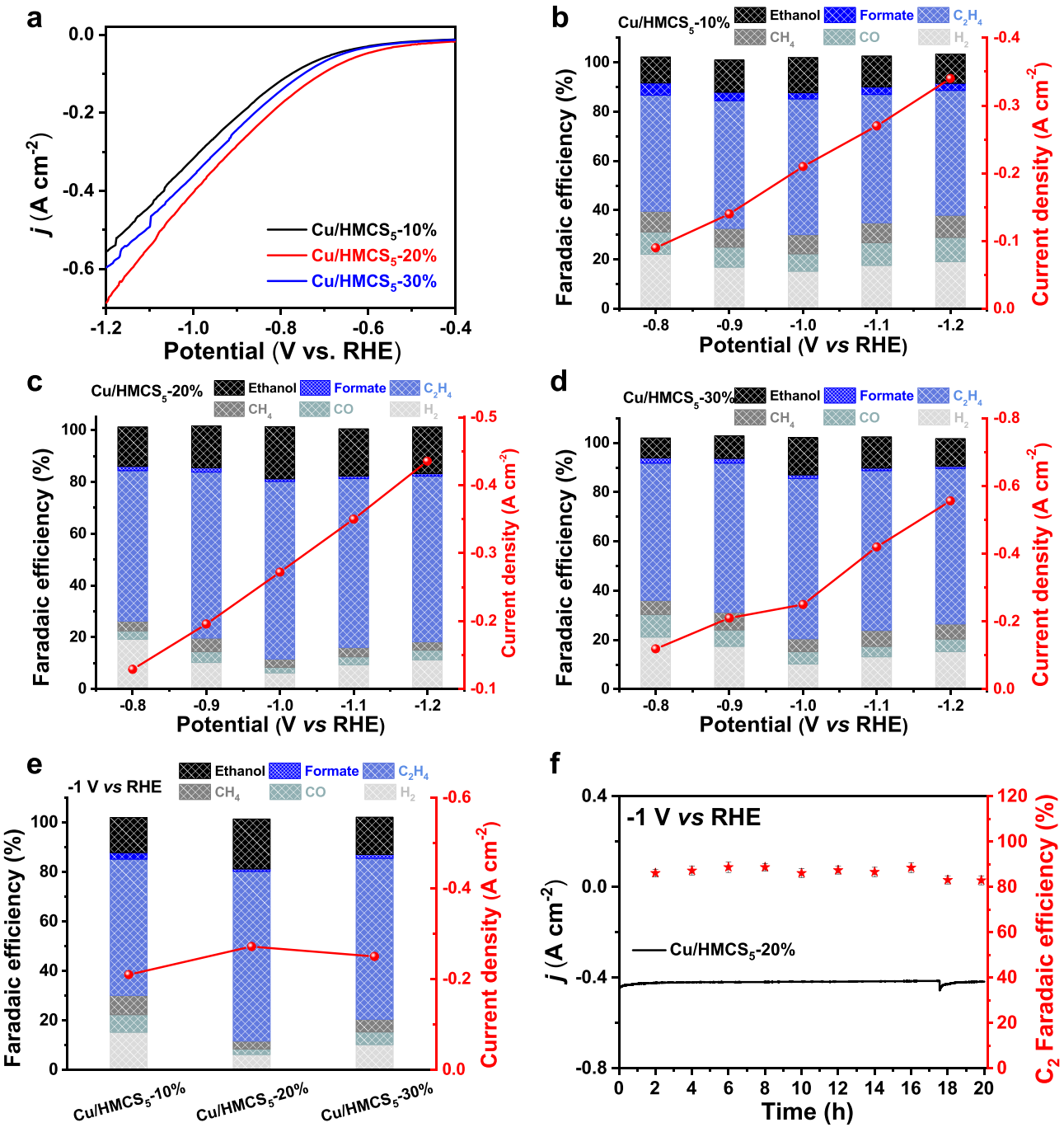

Fig. 3. (a) Comparison of LSV images of the three synthetic materials. (b-d) Total current density and cumulative FEs vs. applied potential in 1 M KOH. (b) Cu/HMCS$_5$-10%. (c) Cu/HMCS$_5$-20%. (d) Cu/HMCS$_5$-30%. (e) FEs of different catalysts at − 1.0 V vs. RHE. (f) Stability test of Cu/HMCS$_5$-20% with C_2 products measured every 7200 s in 1.0 M KOH at − 1.0 V vs. RHE.

the signal of the intermediate *CO. In addition, the signals at 1033 cm^{-1}, 1473 cm^{-1} and 1160 cm^{-1} can be assigned to *CHO, *CH_2O and *OCH_3 respectively, where *CHO is considered to be the key intermediate for CO_2RR [54,56]. The peak at 2986 cm^{-1} is considered to be the characteristic peak for CH_4. As can be seen from Fig. 4a & b, the peak at 1033 cm^{-1} is more pronounced for Cu/HMCS$_5$-20% compared to Cu/HMCS$_5$-10% and is thought to generate more *CHO intermediates. This indicates that the high loading of Cu clusters is more conducive to the formation of *CHO intermediates. Compared to Cu/HMCS$_5$-10% and Cu/HMCS$_5$-20% has weaker peaks for *CH_2O (1473 cm^{-1}), *OCH_3 (1160 cm^{-1}), CH_4 (2986 cm^{-1}) and *COOH (1250 cm^{-1}, 1334 cm^{-1}, 1400 cm^{-1} and 1565 cm^{-1}), indicating that the Cu/HMCS$_5$-10% material loaded with low Cu clusters is more conducive to the adsorption of *CO hydrogenation to CH_4, *CH_2O, *OCH_3 and *COOH. The synergistic effect of Cu atoms in different valence states in the material not only promotes C-C coupling but also stabilizes *OCCO intermediates to form C_2H_4, the conversion of Cu(II) to Cu(I) also facilitates the formation of C_2H_5OH. The nanocavities formed by HMCS are even more favourable for the confinement of the key intermediate *CHO, which favours the formation of C_2H_4 and C_2H_5OH. Cu/HMCS$_5$-30% is also considered to be unfavourable for the conversion of *CO to *CHO intermediates, considering that the material has a smaller ECSA, fewer Cu active sites and reduced nanocavity space compared to Cu/HMCS$_5$-20%.

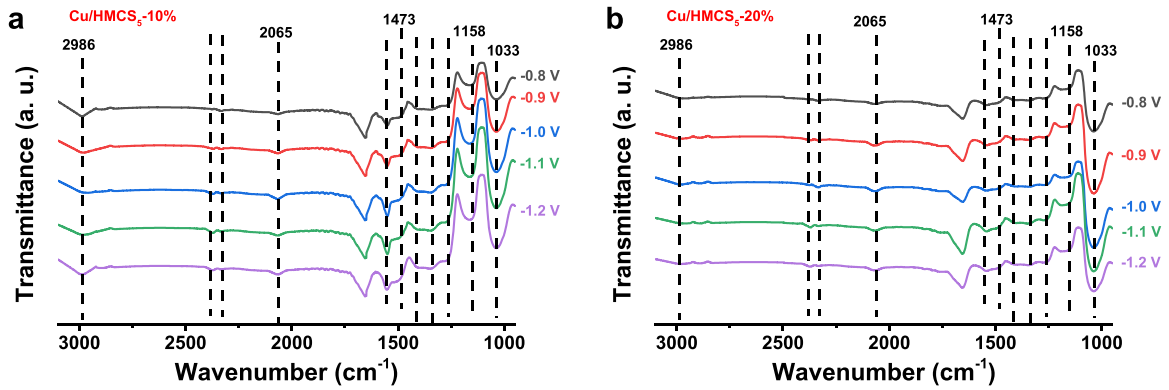

Fig. 4. The in situ FTIRS spectra collected at different applied voltages in a CO_2 saturated 0.1 M $KHCO_3$ electrolyte. (a) Cu/$HMCS_5$-10%. (b) Cu/$HMCS_5$-20%.

4. Conclusions

In summary, a method is proposed to confine and protect Cu clusters in HMCS while forming a confinement effect nanocavity. This can better facilitate the selective production of C_2 from CO_2RR. The C_2 FE of Cu/$HMCS_5$-20% can reach 88.7% at − 1.0 V vs. RHE, with a 68.6% FE for ethylene, which is higher than those of Cu/$HMCS_5$-10% (69.3%, C_2 FE) and Cu/$HMCS_5$-30% (80.1%, C_2 FE). And in comparison with previous reports, Cu/$HMCS_5$-20% also showed the best C_2 selectivity. The reaction process was compared using in situ FTIRS and it was found that the high loading of individual copper atoms confined by HMCS favoured the conversion of *CO to *CHO compared to the Cu/$HMCS_5$-10% material, and the confinement effect of the nanocavity provided by HMCS and the synergistic effect of copper atoms with different valences are beneficial to the formation of C_2H_4 and C_2H_5OH. The method proposed here to improve the C_2 selectivity of CO_2RR using copper clusters confined by HMCSs not only protects the Cu clusters but also provides a confinement effect nanocavity that reduces the amount of Cu. This approach not only develops a new strategy to protect the Cu cluster state and construct confinement effects to improve CO_2RR selectivity, but also provides an attractive way to reduce the amount of Cu used for CO_2 electroreduction into high value-added products.

CRediT authorship contribution statement

Yue Pan: Investigation, Data curation, Conceptualization, Formal analysis, Validation, Writing – original draft. **Hongdong Li**: Formal analysis, Data curation, Validation, Writing – original draft. **Juan Xiong**: Data curation, Conceptualization, Validation. **Yaodong Yu**: Formal analysis. **HaoYang Du**: Validation. **Zhanchao Wu**: Formal analysis. **Shaoxiang Li**: Formal analysis. **Suping Li**: Formal analysis. **Jianping Lai**: Conceptualization, Writing – review & editing, Supervision, Funding acquisition. **Lei Wang**: Writing – review & editing, Funding acquisition, Supervision.

Declaration of Competing Interest

The authors declare that they have no known competing financial interests or personal relationships that could have appeared to influence the work reported in this paper.

Acknowledgement

This work was supported by the National Natural Science Foundation of China (51772162, 22001143, and 52072197), Youth Innovation and Technology Foundation of Shandong Higher Education Institutions, China (2019KJC004), Outstanding Youth Foundation of Shandong Province, China (ZR2019JQ14), Taishan Scholar Young Talent Program (tsqn201909114, tsqn201909123), Natural Science Foundation of Shandong Province (ZR2020YQ34), Major Scientific and Technological Innovation Project (2019JZZY020405), and Major Basic Research Program of Natural Science Foundation of Shandong Province under Grant (ZR2020ZD09).

Appendix A. Supporting information

Supplementary data associated with this article can be found in the online version at doi:10.1016/j.apcatb.2022.121111.

References

[1] M. Zhong, K. Tran, Y. Min, C. Wang, Z. Wang, C.-T. Dinh, P. De Luna, Z. Yu, A. S. Rasouli, P. Brodersen, S. Sun, O. Voznyy, C.-S. Tan, M. Askerka, F. Che, M. Liu, A. Seifitokaldani, Y. Pang, S.-C. Lo, A. Ip, Z. Ulissi, E.H. Sargent, Accelerated discovery of CO_2 electrocatalysts using active machine learning, Nature 581 (2020) 178–183, https://doi.org/10.1038/s41586-020-2242-8.

[2] C. Dinh, T. Burdyny, M.G. Kibria, A. Seifitokaldani, C.M. Gabardo, F.P. García de Arquer, A. Kiani, J.P. Edwards, P. De Luna, O.S. Bushuyev, C. Zou, R. QuinteroBermudez, Y. Pang, D. Sinton, E.H. Sargent, CO_2 electroreduction to ethylene via hydroxide-mediated copper catalysis at an abrupt interface, Science 360 (2018) 783–787. ⟨http://science.sciencemag.org/content/sci/360/6390/783.full.pdf⟩.

[3] H. Zhong, M. GhorbaniAsl, K.H. Ly, J. Zhang, J. Ge, M. Wang, Z. Liao, D. Makarov, E. Zschech, E. Brunner, I.M. Weidinger, J. Zhang, A.V. Krasheninnikov, S. Kaskel, R. Dong, X. Feng, Synergistic electroreduction of carbon dioxide to carbon monoxide on bimetallic layered conjugated metal-organic frameworks, Nat. Commun. 11 (2020) 1409, https://doi.org/10.1038/s41467-020-15141-y.

[4] H. Li, P.H. Opgenorth, D.G. Wernick, S. Rogers, T.-Y. Wu, W. Higashide, P. Malati, Y.-X. Huo, K.M. Cho, J.C. Liao, Integrated electromicrobial conversion of CO_2 to higher alcohols, Science 335 (2012), 1596-1596, ⟨https://www.science.org/cgi/doi/10.1126/science.1217643⟩.

[5] K.U.D. Calvinho, A.B. Laursen, K.M.K. Yap, T.A. Goetjen, S. Hwang, N. Murali, B. Mejia-Sosa, A. Lubarski, K.M. Teeluck, E.S. Hall, E. Garfunkel, M. Greenblatt, G. C. Dismukes, Selective CO_2 reduction to C3 and C4 oxyhydrocarbons on nickel phosphides at overpotentials as low as 10 mV, Energy Environ. Sci. 11 (2018) 2550–2559, https://doi.org/10.1039/C8EE00936H.

[6] M.G. Kibria, C.-T. Dinh, A. Seifitokaldani, P. De Luna, T. Burdyny, R. Quintero-Bermudez, M.B. Ross, O.S. Bushuyev, F.P. García de Arquer, P. Yang, D. Sinton, E. H. Sargent, A surface reconstruction route to high productivity and selectivity in CO_2 electroreduction toward C2+ hydrocarbons, Adv. Mater. 30 (2018), 1804867. ⟨https://onlinelibrary.wiley.com/doi/abs/10.1002/adma.201804867⟩.

[7] S. Liu, X.F. Lu, J. Xiao, X. Wang, X.W. Lou, Bi2O3 Nanosheets grown on multichannel carbon matrix to catalyze efficient CO_2 electroreduction to HCOOH, Angew. Chem. Int. Ed. 58 (2019) 13828–13833. ⟨https://onlinelibrary.wiley.com/doi/abs/10.1002/anie.201907674⟩.

[8] W. Ni, Z. Liu, Y. Zhang, C. Ma, H. Deng, S. Zhang, S. Wang, Electroreduction of carbon dioxide driven by the intrinsic defects in the carbon plane of a single Fe–N4 site, Adv. Mater. 33 (2021), 2003238. ⟨https://onlinelibrary.wiley.com/doi/abs/10.1002/adma.202003238⟩.

[9] H. Li, Y. Han, H. Zhao, W. Qi, D. Zhang, Y. Yu, W. Cai, S. Li, J. Lai, B. Huang, L. Wang, Fast site-to-site electron transfer of high-entropy alloy nanocatalyst driving redox electrocatalysis, Nat. Commun. 11 (2020) 5437, https://doi.org/10.1038/s41467-020-19277-9.

[10] X. Wu, Z. Wang, D. Zhang, Y. Qin, M. Wang, Y. Han, T. Zhan, B. Yang, S. Li, J. Lai, L. Wang, Solvent-free microwave synthesis of ultra-small Ru-Mo2C@CNT with strong metal-support interaction for industrial hydrogen evolution, Nat. Commun. 12 (2021) 4018, https://doi.org/10.1038/s41467-021-24322-2.

[11] N. Nie, D. Zhang, Z. Wang, Y. Qin, X. Zhai, B. Yang, J. Lai, L. Wang, Superfast synthesis of densely packed and ultrafine Pt–lanthanide@KB via solvent-free

microwave as efficient hydrogen evolution electrocatalysts, Small 17 (2021), 2102879. ⟨https://onlinelibrary.wiley.com/doi/abs/10.1002/smll.202102879⟩.
[12] X. Wang, S. Feng, W. Lu, Y. Zhao, S. Zheng, W. Zheng, X. Sang, L. Zheng, Y. Xie, Z. Li, B. Yang, L. Lei, S. Wang, Y. Hou, A new strategy for accelerating dynamic proton transfer of electrochemical CO_2 reduction at high current densities, Adv. Funct. Mater. 31 (2021), 2104243. ⟨https://onlinelibrary.wiley.com/doi/abs/10.1002/adfm.202104243⟩.
[13] Y. Zhang, X. Wang, S. Zheng, B. Yang, Z. Li, J. Lu, Q. Zhang, N.M. Adli, L. Lei, G. Wu, Y. Hou, Hierarchical cross-Linked carbon aerogels with transition metal-nitrogen sites for highly efficient industrial-level CO_2 electroreduction, Adv. Funct. Mater. 31 (2021), 2104377. ⟨https://onlinelibrary.wiley.com/doi/abs/10.1002/adfm.202104377⟩.
[14] W. Zheng, Y. Wang, L. Shuai, X. Wang, F. He, C. Lei, Z. Li, B. Yang, L. Lei, C. Yuan, M. Qiu, Y. Hou, X. Feng, Highly boosted reaction kinetics in carbon dioxide electroreduction by surface-introduced electronegative dopants, Adv. Funct. Mater. 31 (2021), 2008146. ⟨https://onlinelibrary.wiley.com/doi/abs/10.1002/adfm.202008146⟩.
[15] J. Chen, Z. Li, X. Wang, X. Sang, S. Zheng, S. Liu, B. Yang, Q. Zhang, L. Lei, L. Dai, Y. Hou, Promoting CO2 electroreduction kinetics on atomically dispersed monovalent ZnI sites by rationally engineering proton-feeding centers, Angew. Chem. Int. Ed., e202111683. ⟨https://onlinelibrary.wiley.com/doi/abs/10.1002/anie.202111683⟩.
[16] X. Wang, X. Sang, C.-L. Dong, S. Yao, L. Shuai, J. Lu, B. Yang, Z. Li, L. Lei, M. Qiu, L. Dai, Y. Hou, Proton capture strategy for enhancing electrochemical CO_2 reduction on atomically dispersed metal–nitrogen active sites, in: Angew. Chem. Int. Ed, 60, 2021, pp. 11959–11965. ⟨https://onlinelibrary.wiley.com/doi/abs/10.1002/anie.202100011⟩.
[17] X. Chen, J. Chen, N.M. Alghoraibi, D.A. Henckel, R. Zhang, U.O. Nwabara, K. E. Madsen, P.J.A. Kenis, S.C. Zimmerman, A.A. Gewirth, Electrochemical CO_2-to-ethylene conversion on polyamine-incorporated Cu electrodes, Nat. Catal. 4 (2021) 20–27, https://doi.org/10.1038/s41929-020-00547-0.
[18] X. Zhang, J. Li, Y. Li, Y. Jung, Y. Kuang, G. Zhu, Y. Liang, H. Dai, Selective and high current CO_2 electro-reduction to multicarbon products in near-neutral KCl electrolytes, J. Am. Chem. Soc. 143 (2021) 3245–3255, https://doi.org/10.1021/jacs.0c13427.
[19] Y. Duan, F. Meng, K. Liu, S. Yi, S. Li, J. Yan, Q. Jiang, Amorphizing of Cu nanoparticles toward highly efficient and robust electrocatalyst for CO2 reduction to liquid fuels with high faradaic efficiencies, Adv. Mater (2018). ⟨https://onlinelibrary.wiley.com/doi/abs/10.1002/adma.201706194⟩.
[20] L.I. Hung, C. Tsung, W. Huang, P. Yang, Room-temperature formation of hollow Cu2O nanoparticles, Adv. Mater. 22 (2010) 1910–1914, https://doi.org/10.1002/adma.200903947.
[21] W. Zhang, C. Huang, Q. Xiao, L. Yu, L. Shuai, P. An, J. Zhang, M. Qiu, Z. Ren, Y. Yu, Atypical oxygen-bearing copper boosts ethylene selectivity toward electrocatalytic CO_2 reduction, J. Am. Chem. Soc. 142 (2020) 11417–11427, https://doi.org/10.1021/jacs.0c01562.
[22] F. Cui, L. Dou, Q. Yang, Y. Yu, Z. Niu, Y. Sun, H. Liu, A. Dehestani, K. Schierle-Arndt, P. Yang, Benzoin radicals as reducing agent for synthesizing ultrathin copper nanowires, J. Am. Chem. Soc. 139 (2017) 3027–3032, https://doi.org/10.1021/jacs.6b11900.
[23] W. Rong, H. Zou, W. Zang, S. Xi, S. Wei, B. Long, J. Hu, Y. Ji, L. Duan, Size-dependent activity and selectivity of atomic-Level copper nanoclusters during CO/CO_2 electroreduction, Angew. Chem. Int. Ed. 60 (2021) 466–472. ⟨http://www.ncbi.nlm.nih.gov/pubmed/32946193⟩.
[24] B. Zhang, J. Zhang, M. Hua, Q. Wan, Z. Su, X. Tan, L. Liu, F. Zhang, G. Chen, D. Tan, X. Cheng, B. Han, L. Zheng, G. Mo, Highly electrocatalytic ethylene production from CO_2 on nanodefective Cu nanosheets, J. Am. Chem. Soc. 142 (2020) 13606–13613, https://doi.org/10.1021/jacs.0c06420.
[25] K.D. Yang, W.R. Ko, J.H. Lee, S.J. Kim, H. Lee, M.H. Lee, K.T. Nam, Morphology-directed selective production of ethylene or ethane from CO_2 on a Cu mesopore electrode, Angew. Chem. Int. Ed. 56 (2016) 796–800, https://doi.org/10.1002/anie.201610432.
[26] O. Piqué, Q.H. Low, A.D. Handoko, B.S. Yeo, F. Calle-Vallejo, Selectivity map for the late stages of CO and CO_2 reduction to C2 species on copper electrodes, Angew. Chem. Int. Ed. 60 (2021) 10784–10790. ⟨https://onlinelibrary.wiley.com/doi/abs/10.1002/anie.202014060⟩.
[27] Y. Zhong, Y. Xu, J. Ma, C. Wang, S. Sheng, C. Cheng, M. Li, L. Han, L. Zhou, Z. Cai, Y. Kuang, Z. Liang, X. Sun, An artificial electrode/electrolyte interface for CO_2 electroreduction by cation surfactant self-assembly, Angew. Chem. Int. Ed. 59 (2020) 19095–19101. ⟨https://onlinelibrary.wiley.com/doi/abs/10.1002/anie.202005522⟩.
[28] Z.-Q. Liang, T.-T. Zhuang, A. Seifitokaldani, J. Li, C.-W. Huang, C.-S. Tan, Y. Li, P. De Luna, C.T. Dinh, Y. Hu, Q. Xiao, P.-L. Hsieh, Y. Wang, F. Li, R. Quintero-Bermudez, Y. Zhou, P. Chen, Y. Pang, S.-C. Lo, L.-J. Chen, H. Tan, Z. Xu, S. Zhao, D. Sinton, E.H. Sargent, Copper-on-nitride enhances the stable electrosynthesis of multi-carbon products from CO_2, Nat. Commun. 9 (2018) 3828, https://doi.org/10.1038/s41467-018-06311-0.
[29] J. Li, F. Che, Y. Pang, C. Zou, J.Y. Howe, T. Burdyny, J.P. Edwards, Y. Wang, F. Li, Z. Wang, P. De Luna, C.-T. Dinh, T.-T. Zhuang, M.I. Saidaminov, S. Cheng, T. Wu, Y.Z. Finfrock, L. Ma, S.-H. Hsieh, Y.-S. Liu, G.A. Botton, W.-F. Pong, X. Du, J. Guo, T.-K. Sham, E.H. Sargent, D. Sinton, Copper adparticle enabled selective electrosynthesis of n-propanol, Nat. Commun. 9 (2018) 4614, https://doi.org/10.1038/s41467-018-07032-0.
[30] Q. Zhu, X. Sun, D. Yang, J. Ma, X. Kang, L. Zheng, J. Zhang, Z. Wu, B. Han, Carbon dioxide electroreduction to C2 products over copper-cuprous oxide derived from electrosynthesized copper complex, Nat. Commun. 10 (2019) 3851, https://doi.org/10.1038/s41467-019-11599-7.
[31] P. Iyengar, M.J. Kolb, J.R. Pankhurst, F. Calle-Vallejo, R. Buonsanti, Elucidating the facet-dependent selectivity for CO_2 electroreduction to ethanol of Cu–Ag tandem catalysts, ACS Catal. (2021) 4456–4463, https://doi.org/10.1021/acscatal.1c00420.
[32] H.-Q. Liang, S. Zhao, X.-M. Hu, M. Ceccato, T. Skrydstrup, K. Daasbjerg, Hydrophobic copper interfaces boost electroreduction of carbon dioxide to ethylene in water, ACS Catal. 11 (2021) 958–966, https://doi.org/10.1021/acscatal.0c03766.
[33] M.S. Xie, B.Y. Xia, Y. Li, Y. Yan, Y. Yang, Q. Sun, S.H. Chan, A. Fisher, X. Wang, Amino acid modified copper electrodes for the enhanced selective electroreduction of carbon dioxide towards hydrocarbons, Energy Environ. Sci. 9 (2016) 1687–1695, https://doi.org/10.1039/C5EE03694A.
[34] T.-T. Zhuang, Z.-Q. Liang, A. Seifitokaldani, Y. Li, P. De Luna, T. Burdyny, F. Che, F. Meng, Y. Min, R. Quintero-Bermudez, C.T. Dinh, Y. Pang, M. Zhong, B. Zhang, J. Li, P.-N. Chen, X.-L. Zheng, H. Liang, W.-N. Ge, B.-J. Ye, D. Sinton, S.-H. Yu, E. H. Sargent, Steering post-C–C coupling selectivity enables high efficiency electroreduction of carbon dioxide to multi-carbon alcohols, Nat. Catal. 1 (2018) 421–428, https://doi.org/10.1038/s41929-018-0084-7.
[35] R. Kas, K.K. Hummadi, R. Kortlever, P. de Wit, A. Milbrat, M.W.J. Luiten-Olieman, N.E. Benes, M.T.M. Koper, G. Mul, Three-dimensional porous hollow fibre copper electrodes for efficient and high-rate electrochemical carbon dioxide reduction, Nat. Commun. 7 (2016) 10748, https://doi.org/10.1038/ncomms10748.
[36] D. Kim, J. Resasco, Y. Yu, A.M. Asiri, P. Yang, Synergistic geometric and electronic effects for electrochemical reduction of carbon dioxide using gold–copper bimetallic nanoparticles, Nat. Commun. 5 (2014) 4948, https://doi.org/10.1038/ncomms5948.
[37] T. Kim, G.T.R. Palmore, A scalable method for preparing Cu electrocatalysts that convert CO_2 into C2+ products, Nat. Commun. 11 (2020) 3622, https://doi.org/10.1038/s41467-020-16998-9.
[38] H. Zhao, D. Zhang, Z. Wang, Y. Han, X. Sun, H. Li, X. Wu, Y. Pan, Y. Qin, S. Lin, Z. Xu, J. Lai, L. Wang, High-performance nitrogen electroreduction at low overpotential by introducing Pb to Pd nanosponges, Appl. Catal. B 265 (2020), 118481. ⟨https://www.sciencedirect.com/science/article/pii/S0926337319312275⟩.
[39] J. Pan, Y. Sun, P. Deng, F. Yang, S. Chen, Q. Zhou, H.S. Park, H. Liu, B. Yu Xia, Hierarchical and ultrathin copper nanosheets synthesized via galvanic replacement for selective electrocatalytic carbon dioxide conversion to carbon monoxide, Appl. Catal. B 255 (2019), 117736. ⟨http://www.sciencedirect.com/science/article/pii/S0926337319304758⟩.
[40] L. Dai, Q. Qin, P. Wang, X. Zhao, C. Hu, P. Liu, R. Qin, M. Chen, D. Ou, C. Xu, S. Mo, B. Wu, G. Fu, P. Zhang, N. Zheng, Ultrastable atomic copper nanosheets for selective electrochemical reduction of carbon dioxide, Sci. Adv. 3 (2017), e1701069, https://doi.org/10.1126/sciadv.1701069#.
[41] X. Yuan, S. Chen, D. Cheng, L. Li, W. Zhu, D. Zhong, Z.-J. Zhao, J. Li, T. Wang, J. Gong, Controllable Cu0-Cu+ sites for electrocatalytic reduction of carbon dioxide, Angew. Chem. Int. Ed. 60 (2021) 15344–15347. ⟨https://onlinelibrary.wiley.com/doi/abs/10.1002/anie.202105118⟩.
[42] Z. Lyu, S. Zhu, M. Xie, Y. Zhang, Z. Chen, R. Chen, M. Tian, M. Chi, M. Shao, Y. Xia, Controlling the surface oxidation of Cu nanowires improves their catalytic selectivity and stability toward C2+ products in CO2 reduction, Angew. Chem. Int. Ed (2021) 1909–1915. ⟨https://onlinelibrary.wiley.com/doi/abs/10.1002/anie.202011956⟩.
[43] Y. Zhou, F. Che, M. Liu, C. Zou, Z. Liang, P. De Luna, H. Yuan, J. Li, Z. Wang, H. Xie, H. Li, P. Chen, E. Bladt, R. QuinteroBermudez, T. Sham, S. Bals, J. Hofkens, D. Sinton, G. Chen, E.H. Sargent, Dopant-induced electron localization drives CO_2 reduction to C2 hydrocarbons, Nat. Chem. 10 (2018) 974–980, https://doi.org/10.1038/s41557-018-0092-x.
[44] G. Majano, J. Pérez-Ramírez, Scalable room-temperature conversion of copper (II) hydroxide into HKUST-1 (Cu3(btc)2, Adv. Mater. 25 (2013) 1052–1057, https://doi.org/10.1002/adma.201203664.
[45] K.-L. Bae, J. Kim, C.K. Lim, K.M. Nam, H. Song, Colloidal zinc oxide-copper(I) oxide nanocatalysts for selective aqueous photocatalytic carbon dioxide conversion into methane, Nat. Commun. 8 (2017) 1156, https://doi.org/10.1038/s41467-017-01165-4.
[46] X. Wang, K. Klingan, M. Klingenhof, T. Möller, J. Ferreira de Araújo, I. Martens, A. Bagger, S. Jiang, J. Rossmeisl, H. Dau, P. Strasser, Morphology and mechanism of highly selective Cu(II) oxide nanosheet catalysts for carbon dioxide electroreduction, Nat. Commun. 12 (2021) 794, https://doi.org/10.1038/s41467-021-20961-7.
[47] J. Wang, T. Cheng, A.Q. Fenwick, T.N. Baroud, A. Rosas-Hernández, J.H. Ko, Q. Gan, W.A. Goddard Iii, R.H. Grubbs, Selective CO_2 electrochemical reduction enabled by a tricomponent copolymer modifier on a copper surface, J. Am. Chem. Soc. 143 (2021) 2857–2865, https://doi.org/10.1021/jacs.0c12478.
[48] P.-P. Yang, X.-L. Zhang, F.-Y. Gao, Y.-R. Zheng, Z.-Z. Niu, X. Yu, R. Liu, Z.-Z. Wu, S. Qin, L.-P. Chi, Y. Duan, T. Ma, X.-S. Zheng, J.-F. Zhu, H.-J. Wang, M.-R. Gao, S.-H. Yu, Protecting copper oxidation state via intermediate confinement for selective CO_2 electroreduction to C2+ fuels, J. Am. Chem. Soc. 142 (2020) 6400–6408, https://doi.org/10.1021/jacs.0c01699.
[49] T.-T. Zhuang, Y. Pang, Z.-Q. Liang, Z. Wang, Y. Li, C.-S. Tan, J. Li, C.T. Dinh, P. De Luna, P.-L. Hsieh, T. Burdyny, H.-H. Li, M. Liu, Y. Wang, F. Li, A. Proppe, A. Johnston, D.-H. Nam, Z.-Y. Wu, Y.-R. Zheng, A.H. Ip, H. Tan, L.-J. Chen, S.-H. Yu, S.O. Kelley, D. Sinton, E.H. Sargent, Copper nanocavities confine intermediates for efficient electrosynthesis of C3 alcohol fuels from carbon

monoxide, Nat. Catal. 1 (2018) 946–951, https://doi.org/10.1038/s41929-018-0168-4.
[50] C. Liu, M. Zhang, J. Li, W. Xue, T. Zheng, C. Xia, J. Zeng, Nanoconfinement engineering over hollow multi-shell structured copper towards efficient electrocatalytical C-C coupling, Angew. Chem. Int. Ed., ⟨https://onlinelibrary.wiley.com/doi/abs/10.1002/anie.202113498⟩.
[51] W. Xiong, H. Li, H. You, M. Cao, R. Cao, Encapsulating metal organic framework into hollow mesoporous carbon sphere as efficient oxygen bifunctional electrocatalyst, Natl. Sci. Rev. 7 (2019) 609–619, https://doi.org/10.1093/nsr/nwz166.
[52] X.K. Wan, H.B. Wu, B.Y. Guan, D. Luan, X.W.D. Lou, Confining sub-nanometer Pt clusters in hollow mesoporous carbon spheres for boosting hydrogen evolution activity, Adv. Mater. 32 (2020), e1901349. ⟨http://www.ncbi.nlm.nih.gov/pubmed/31879997⟩.
[53] Z. Wu, Y. Li, J. Liu, Z. Lu, H. Zhang, B. Yang, Colloidal self-assembly of catalytic copper nanoclusters into ultrathin ribbons, Angew. Chem. Int. Ed. 53 (2014) 12196–12200, https://doi.org/10.1002/anie.201407390.
[54] J.-D. Yi, R. Xie, Z.-L. Xie, G.-L. Chai, T.-F. Liu, R.-P. Chen, Y.-B. Huang, R. Cao, Highly selective CO_2 electroreduction to CH4 by in-situ generated Cu2O single-type sites on a conductive MOF: Stabilizing key intermediates with hydrogen bonding, Angew. Chem. Int. Ed. 59 (2020) 23641–23648. ⟨https://onlinelibrary.wiley.com/doi/abs/10.1002/anie.202010601⟩.
[55] Y. Zou, S. Wang, An investigation of active sites for electrochemical CO_2 reduction reactions: from in situ characterization to rational design, Adv. Sci. 8 (2021), 2003579. ⟨https://onlinelibrary.wiley.com/doi/abs/10.1002/advs.202003579⟩.
[56] Y. Zheng, A. Vasileff, X. Zhou, Y. Jiao, M. Jaroniec, S.-Z. Qiao, Understanding the roadmap for electrochemical reduction of CO_2 to multi-carbon oxygenates and hydrocarbons on copper-based catalysts, J. Am. Chem. Soc. 141 (2019) 7646–7659, https://doi.org/10.1021/jacs.9b02124.